NASA/TM—2012-216029

Charpy Impact Energy and Microindentation Hardness of 60-NITINOL

Malcolm K. Stanford
Glenn Research Center, Cleveland, Ohio

September 2012

NASA STI Program . . . in Profile

Since its founding, NASA has been dedicated to the advancement of aeronautics and space science. The NASA Scientific and Technical Information (STI) program plays a key part in helping NASA maintain this important role.

The NASA STI Program operates under the auspices of the Agency Chief Information Officer. It collects, organizes, provides for archiving, and disseminates NASA's STI. The NASA STI program provides access to the NASA Aeronautics and Space Database and its public interface, the NASA Technical Reports Server, thus providing one of the largest collections of aeronautical and space science STI in the world. Results are published in both non-NASA channels and by NASA in the NASA STI Report Series, which includes the following report types:

- TECHNICAL PUBLICATION. Reports of completed research or a major significant phase of research that present the results of NASA programs and include extensive data or theoretical analysis. Includes compilations of significant scientific and technical data and information deemed to be of continuing reference value. NASA counterpart of peer-reviewed formal professional papers but has less stringent limitations on manuscript length and extent of graphic presentations.

- TECHNICAL MEMORANDUM. Scientific and technical findings that are preliminary or of specialized interest, e.g., quick release reports, working papers, and bibliographies that contain minimal annotation. Does not contain extensive analysis.

- CONTRACTOR REPORT. Scientific and technical findings by NASA-sponsored contractors and grantees.

- CONFERENCE PUBLICATION. Collected papers from scientific and technical conferences, symposia, seminars, or other meetings sponsored or cosponsored by NASA.

- SPECIAL PUBLICATION. Scientific, technical, or historical information from NASA programs, projects, and missions, often concerned with subjects having substantial public interest.

- TECHNICAL TRANSLATION. English-language translations of foreign scientific and technical material pertinent to NASA's mission.

Specialized services also include creating custom thesauri, building customized databases, organizing and publishing research results.

For more information about the NASA STI program, see the following:

- Access the NASA STI program home page at *http://www.sti.nasa.gov*

- E-mail your question to *help@sti.nasa.gov*

- Fax your question to the NASA STI Information Desk at 443–757–5803

- Phone the NASA STI Information Desk at 443–757–5802

- Write to:
  STI Information Desk
  NASA Center for AeroSpace Information
  7115 Standard Drive
  Hanover, MD 21076–1320

NASA/TM—2012-216029

Charpy Impact Energy and Microindentation Hardness of 60-NITINOL

Malcolm K. Stanford
Glenn Research Center, Cleveland, Ohio

National Aeronautics and
Space Administration

Glenn Research Center
Cleveland, Ohio 44135

September 2012

Acknowledgments

Thank you to Joy A. Buehler, Dereck F. Johnson, Terry R. McCue, Richard B. Rogers, Fransua Thomas and Walter A. Wozniak for their technical assistance during this study and to Dr. Christopher DellaCorte for helpful technological discussions.

This report contains preliminary findings, subject to revision as analysis proceeds.

Level of Review: This material has been technically reviewed by technical management.

Available from

NASA Center for Aerospace Information
7115 Standard Drive
Hanover, MD 21076–1320

National Technical Information Service
5301 Shawnee Road
Alexandria, VA 22312

Available electronically at http://www.sti.nasa.gov

Charpy Impact Energy and Microindentation Hardness of 60-NITINOL

Malcolm K. Stanford
National Aeronautics and Space Administration
Glenn Research Center
Cleveland, Ohio 44135

Abstract

60-NITINOL (60 wt.% Ni – 40 wt.% Ti) is being studied as a material for advanced aerospace components. The Charpy impact energy and microindentation hardness has been studied for this material, fabricated by vacuum induction skull melting (casting) and by hot isostatic pressing. Test specimens were prepared in various hardened and annealed heat treatment conditions. The average impact energy ranged from 0.33 to 0.49 J for the hardened specimens while the annealed specimens had impact energies ranging from 0.89 to 1.18 J. The average hardness values of the hardened specimens ranged from 590 to 676 HV while that of the annealed specimens ranged from 298 to 366 HV, suggesting an inverse relationship between impact energy and hardness. These results are expected to provide guidance in the selection of heat treatment processes for the design of mechanical components.

Introduction

The topic of impact toughness rose to prominence after the sinking of the Royal Mail Steamship *Titanic*. The forward starboard hull of the ship struck an iceberg at about 11:40 p.m. on the night of April 15, 1912, resulting in the sinking of the ship in approximately two and a half hours (Ref. 1). Though the ship was thought by many to be unsinkable, its designers were apparently unaware of a basic, intrinsic materials property, namely, the ductile-to-brittle transition temperature. The icy waters of the Atlantic embrittled the crystallographically body-centered cubic (bcc) iron of the ship's hull, reducing its impact energy (Ref. 2). Unfortunately, the human drive for exploration and progress has had a number of monumental disasters that, while paralleled by some as the inevitable result of Homerian hubris (Ref. 3), have alternatively served as educational opportunities to enable future progress.

In the century that has passed since the fateful first voyage of the *Titanic*, a great deal of effort has been focused on studying the response of materials to impact loading. It is now well-known that the body-centered cubic crystal structure has fewer slip systems than the face-centered cubic system, reducing the ability of the bcc system to deform prior to fracture and making it particularly susceptible to a transition to brittle fracture at lower temperatures. Lots of ongoing work is focused on understanding the behavior of ship hull materials under dynamic loads (Refs. 4 to 6). Similarly, there are many investigations on the response of jet engine and airframe structural materials to foreign object damage (Refs. 7 to 9).

Impact damage is certainly a concern in crewed space vehicles (Refs. 10 and 11). However, internal components must also be able to withstand shock loads due to high g-force-induced vibration during launch, especially in un-crewed vehicles where g-forces can become very high. The National Aeronautics and Space Administration is currently studying 60-NITINOL for incorporation in aerospace gears and bearings. 60-NITINOL is an ordered intermetallic material consisting of 60wt%Ni and 40wt%Ti (Ref. 12). This material is of interest to the aerospace community because it is corrosion-resistant, has moderate density, can be easily hardened for wear resistance and because it is superelastic, capable of recoverable elastic strains nearly ten times those of conventional materials (Ref. 13). However, as with most intermetallics, this material is inherently brittle. 60-NITINOL has the B2 crystal structure, very similar to the bcc crystal structure, with Ni atoms at the eight corners of the unit cell and Ti at the body-centered position. The lack of available slip systems and the rigid arrangement of atoms in this material are the underlying (atomic-scale) reasons for its brittle behavior. However, the mechanisms that allow brittle failure to initiate on the micro-scale should be understood so that methods to reduce or prevent these types of failures may be developed.

The focus of this investigation was to identify the failure mechanisms of this material in various heat treatment conditions when subjected to impact loading. While mechanical tests are helpful for the specification of an operating environment, these tests typically only apply static loads to the material, where actual components are often subjected to dynamic loads. These results will provide a conservative estimation of the behavior of this material in lieu of forthcoming static compression strength and fracture toughness evaluations.

Materials and Procedures

60-NITINOL (nominal composition: 60wt% Ni - 40wt% Ti) was obtained from commercial sources, fabricated by the following methods:

1. *Vacuum induction skull melting* of bulk 60-NITINOL with a water-cooled copper crucible. This method is

hereafter referred to as *casting* (resulting in *cast material*). The cast material was subsequently hot isostatically pressed for 2 hr at 900 °C and 100 MPa to diminish porosity. The materials from these two heats are hereafter designated "Cast-A" and "Cast-B" material.

2. *Hot isostatic pressing (HIPping)* of gas atomized 60-NITINOL powder. This method is henceforth referred to as the powder metallurgy (or PM) method (resulting in *PM material*). The two ingots of material fabricated by this technique that were used in this study were obtained from two different suppliers using proprietary techniques. The materials from these two ingots are subsequently identified as "PM-X" and "PM-Y" material.

The chemical compositions of the materials used in this study were analyzed by inductively-coupled plasma optical emission spectroscopy (ICP-OES).

Specimens for Charpy impact testing, depicted schematically in Figure 1, were cut from the ingots by wire electrical-discharge machining (EDM). The specimens were heat treated by *water-quenched*, *aged* or *furnace-cooled* heat treatments as listed in Table I, and then tested as specified in ASTM E23-07a$^{\varepsilon 1}$ (Ref. 14). The Charpy impact test measures the energy required to fracture a specimen by determining the difference between the initial height *h* and final height *h'* of a hammer (or striker) on a pendulum when it impacts a specimen of the studied material. The setup used in this study is depicted schematically in Figure 2. Three to four replicate specimens with each of the specified heat treatment conditions were tested at room temperature on an apparatus designed to measure impact energies from 0 to 2.82 J (0 to 25 in.-lb) with 0.028 J (0.25 in.-lb) divisions. The speed of the striker at impact was approximately 3.46 m/s. The striker profile used for these tests had a radius of 8 mm and the chordal distance of this radius was approximately 4 mm. After testing, the fractured surfaces of the specimens were examined by scanning electron microscopy (SEM) and by energy-dispersive x-ray spectroscopy (EDS).

Cross sections of specimens were sectioned perpendicular to the direction of crack propagation with an abrasive cut-off saw using a resin bonded aluminum oxide blade. The wheel rotated at 3820 rpm and was set to have a traverse speed of 0.1 mm/s.

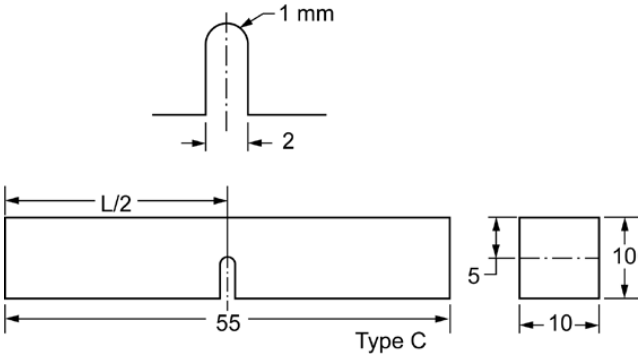

Figure 1.—Schematic of Charpy U-notch specimen used in this investigation.

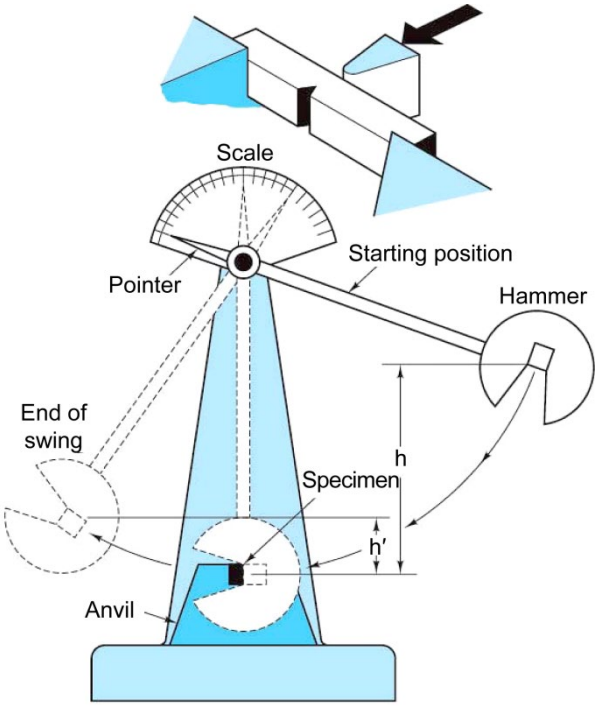

Figure 2.—Schematic representation of Charpy test of impact energy (Ref. 17).

TABLE I.—HEAT TREATMENT CONDITIONS USED ON CHARPY SPECIMENS IN THIS STUDY

Designation	Heat treatment for cast material	Heat treatment for PM material
Water-quenched (partially solution treated)	[a]90 min at 980 °C/water quench (WQ)	[a]60 min at 1000 °C/WQ
Aged (water-quenched and aged)	90 min at 980 °C/WQ/60 min at 400°C/WQ	60 min at 1000 °C/WQ/60 min at 400 °C/WQ
Furnace-cooled	[b]70 min at 1040 °C/furnace cool (FC)	[b]120 min at 1000 °C/FC

[a]Water quenching was done in still room temperature water. The specimen was swirled about in the water.
[b]Furnace cooling was done by shutting off the power to the furnace after the specified heat soak and allowing it to cool to room temperature, which took approximately 24 hr.

The specimens were prepared for microstructural examination using standard metallographic procedures. A total of approximately 1 mm of each specimen was removed from the sectioned surface during the grinding and polishing procedure. The final polish used colloidal silica on a vibratory polisher. The microindentation hardness was measured with a standard technique using a Vickers (pyramidal) diamond indenter with a 500 gf load and a load apply of approximately 12 s (Ref. 15). The polished cross sections were then swab-etched with a 1vol%HF-10vol%HNO_3 solution in deionized water and then examined with an optical microscope.

Results and Discussion

The results of the chemical analysis are listed in Table II. The composition of each of the studied specimens was nominally 60wt%Ni and 40wt%Ti with oxygen, iron, copper and aluminum making up the primary impurities. Due to the high reactivity of titanium at high temperatures, some of the oxygen was likely adsorbed during primary metallurgical processing. In addition, some of the aluminum, copper and oxygen are probably the result of low-level contamination from alumina- and copper-based melting equipment.

TABLE II.—NOMINAL COMPOSITIONS OF THE STUDIED SPECIMENS

Identification	Composition	Impurities, ppm
Cast-A	59.6wt%Ni-40.3wt%Ti	O (680), Fe (130), Al (200), N (40), Co (30), Cr (20)
Cast-B	60.1wt%Ni-39.8wt%Ti	O (640), Fe (430), Al (200), N (70), Cu (250), Co (25), Zr (30), V (25), Mn (4)
PM-X	59.4wt%Ni-40.5wt%Ti	O (580), Fe (100), Al (80), Cu (90), Cr (20), Co (5)
PM-Y	60.5wt%Ni-39.4wt%Ti	O (395), Fe (130), Al (90), Cr (35), N (30)

Fractography

The fracture surfaces of the furnace-cooled specimens had a dull appearance when observed with the unaided eye. As shown in Figure 3, under SEM observation the fracture surfaces had a grainy texture, which is characteristic of intergranular fracture. There was no discernable fracture initiation site for these specimens. At high-magnification (Figure 4, Figure 5 and Figure 6), the fracture surface is faceted and clearly indicative of brittle intergranular fracture. Observation of the polished cross sections, as shown in Figure 7 and Figure 8, showed that the fracture tended to follow the second phase Ni_3Ti that typically decorates the grain boundaries of this material, further indicating that fracture was intergranular.

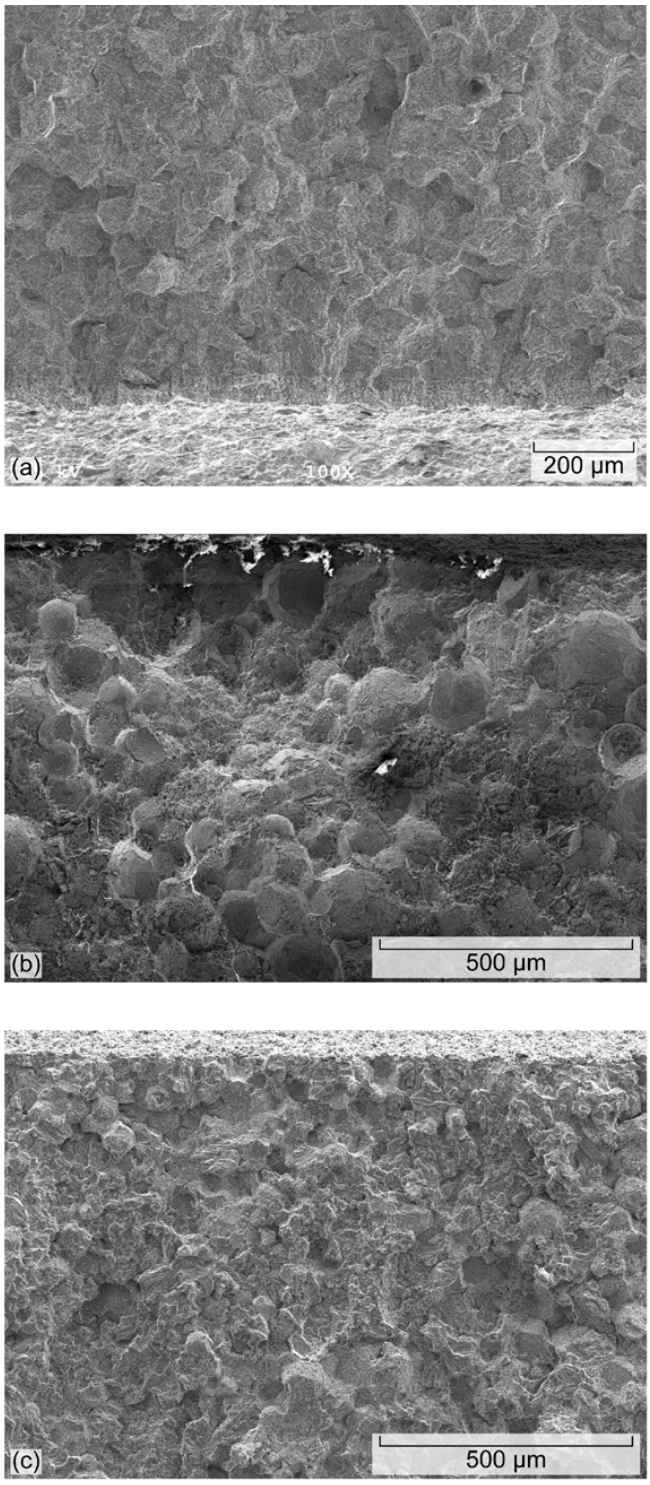

Figure 3.—SEM photomicrographs of representative fracture surfaces for (a) Cast-A, (b) PM-X and (c) PM-Y 60-NITINOL materials in the furnace-cooled heat treatment condition showing intergranular fracture.

The fracture surface of a PM-X specimen (see Figure 5) shows unconsolidated spherical particles and depressions at the prior locations of unconsolidated particles. Examination of cross sections by optical microscopy (shown in Figure 7) corroborated this finding. Unconsolidated particles are thought to be a result of particles that were slightly oxidized during the atomization process. Work is underway to determine if this problem can be mitigated with this material through some combination of higher HIP temperatures and cycle times to force the oxide layer to diffuse away from the particle boundaries. It is possible that this issue can be eliminated with tighter control of the atomization chamber atmosphere to prevent the oxidation in the first place. However, when even small amounts of oxygen come into contact with a high surface area powder with an oxygen-solvent like Ti, the kinetics driving the formation of oxides would be very strong. Notwithstanding, PM-Y specimens showed no indications of unconsolidated particles.

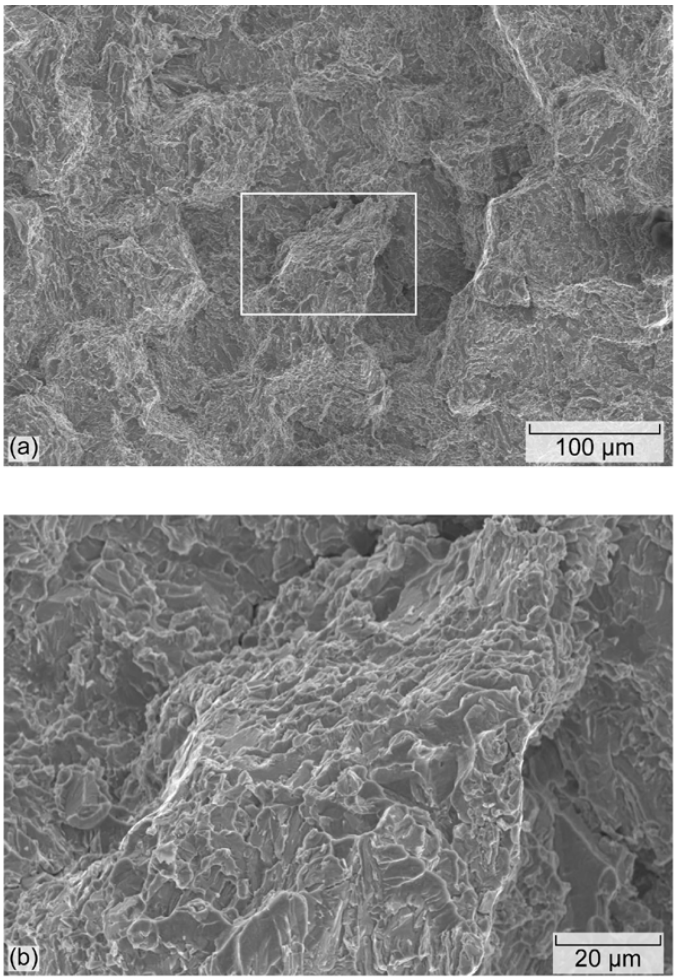

Figure 4.—(a) The fracture surface of a Cast-A Charpy specimen in the furnace-cooled heat treatment condition (the highlighted area in (a) is shown at higher magnification in (b)). While there is no clear fracture initiation site, the brittle nature of the fracture is apparent from the sharp, faceted surface morphology.

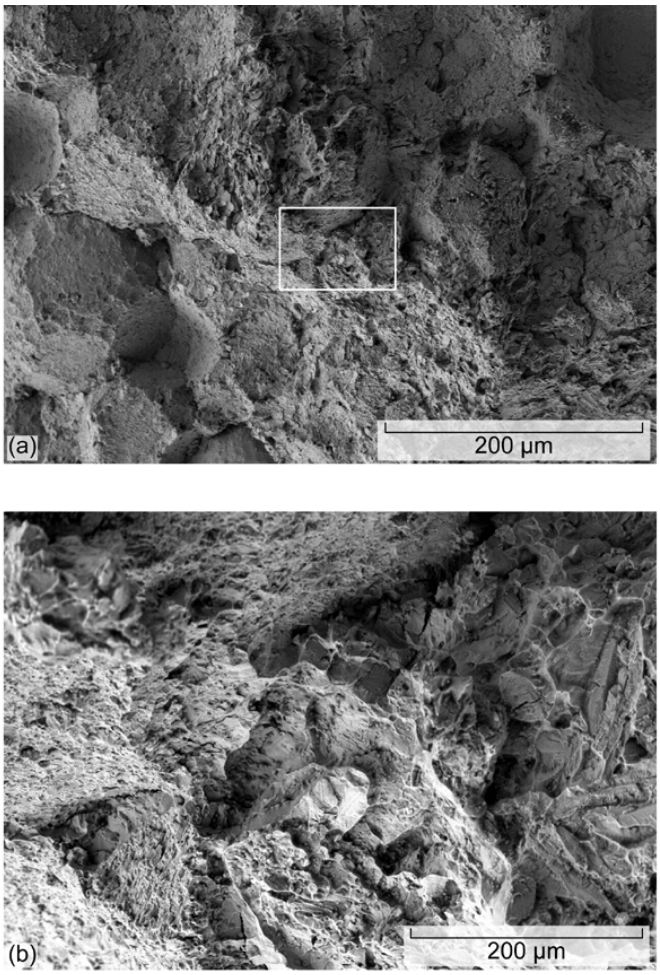

Figure 5.—The fracture surface of a PM-X Charpy specimen in the furnace-cooled heat treatment condition (the highlighted area in (a) is shown at higher magnification in (b)). While there is no clear fracture initiation site, the brittle nature of the fracture is apparent from the sharp, faceted surface morphology.

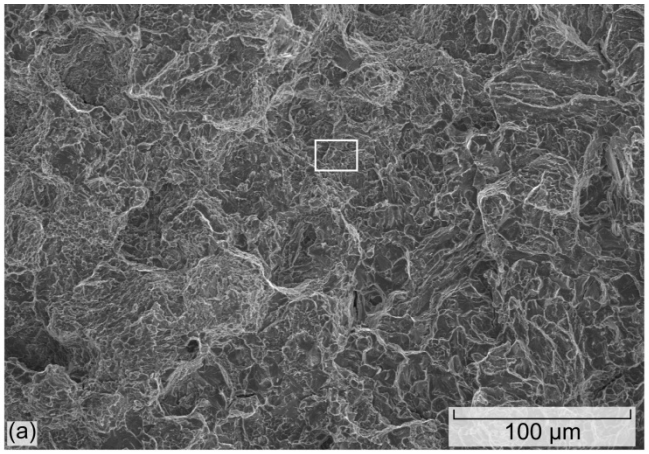

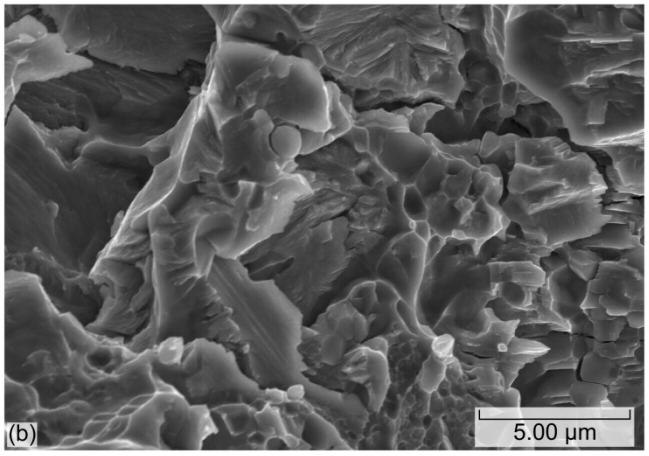

Figure 6.—The fracture surface of a PM-Y Charpy specimen in the furnace-cooled heat treatment condition (the highlighted area in (a) is shown at higher magnification in (b)). While there is no clear fracture initiation site, the brittle nature of the fracture is apparent from the sharp, faceted surface morphology.

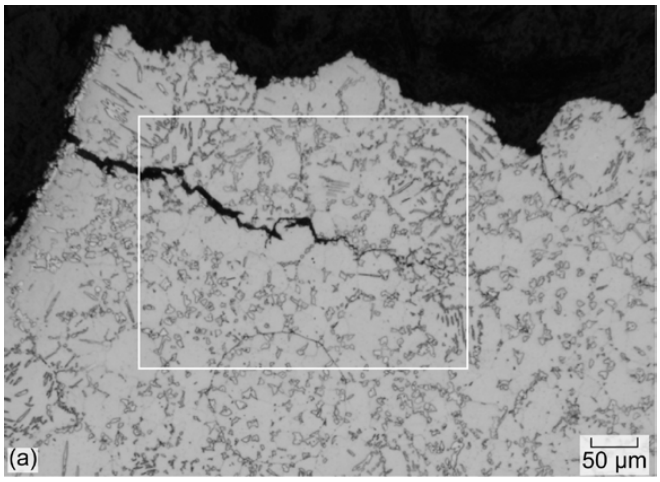

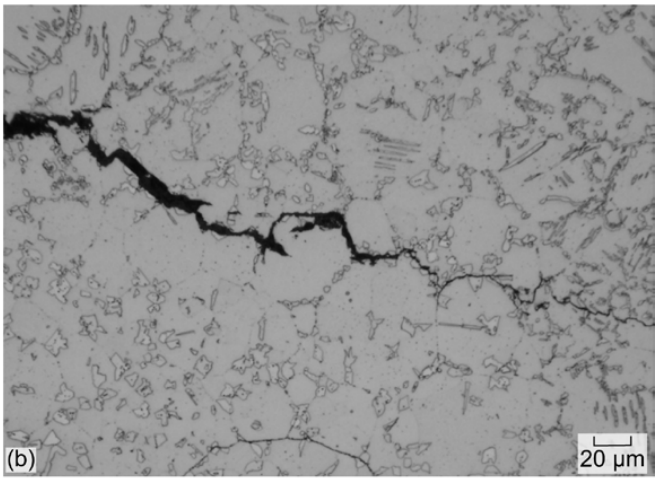

Figure 7.—Cross-sectional image through the U-notch in furnace-cooled PM-X material showing intergranular fracture (IGF) and unconsolidated particles (U). The rectangle in (a) indicates the proximal area shown at higher magnification in (b).

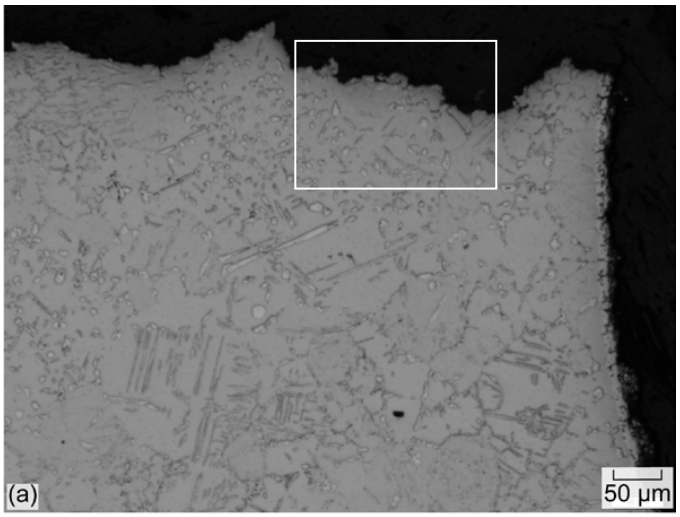

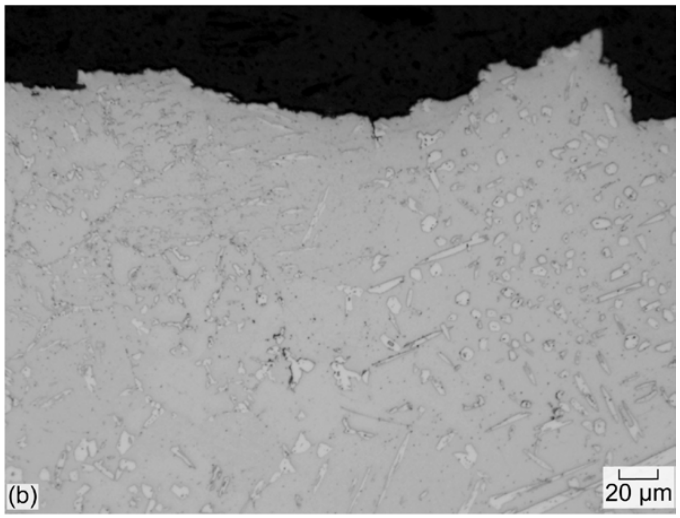

Figure 8.—Optical photomicrograph of a cross-section (a) through the U-notch of a furnace-cooled PM-Y specimen and (b) at higher magnification showing intergranular fracture (second phase Ni_3Ti decorates the fracture path along the top edge of the specimen).

The fracture surfaces of the water-quenched specimens were shiny to the naked eye. Observation by SEM revealed classical chevron patterns resulting from brittle fracture, which can be seen in Figure 9(a) to (c). The fracture origins (labeled "FO") were determined by following the direction of crack propagation in reverse.

The fracture origins in Cast-A specimens had particulate contamination, as shown in Figure 10. Upon examination by EDS (see Figure 10(d)), the particles were found to consist of Zr and O. Further investigation determined that the contaminant was zirconia (ZrO_2), which had been used as part of a crucible lining during the casting process (Ref. 16). Cast-B material was melted in a crucible without this zirconia liner.

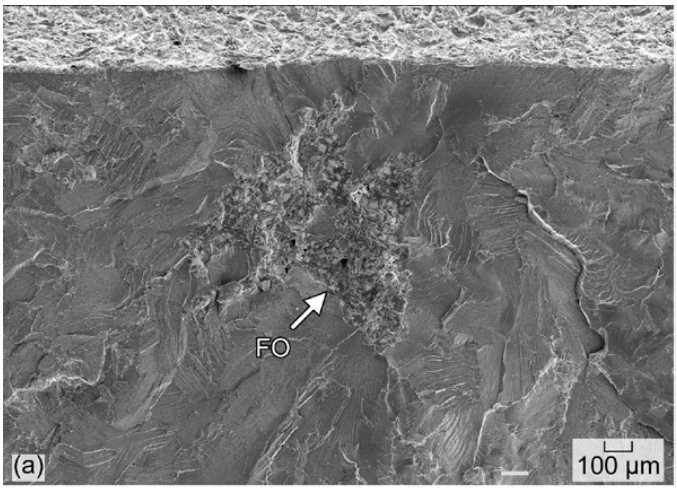

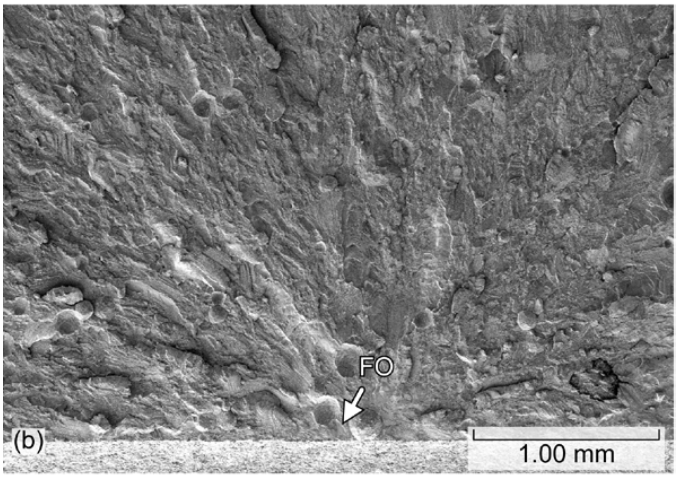

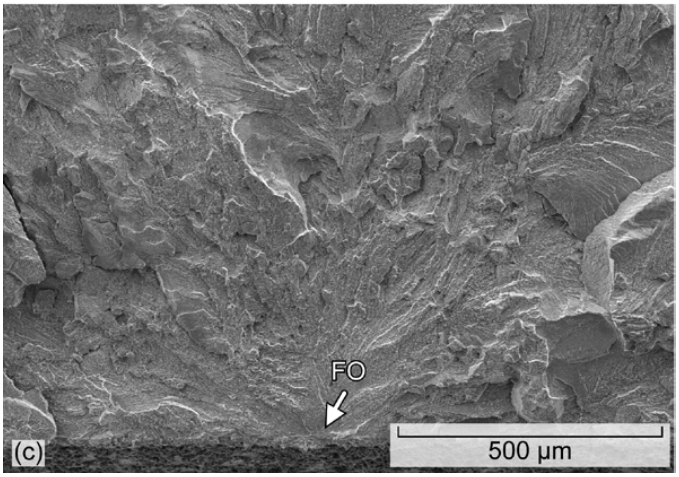

Figure 9.—SEM photomicrographs of representative fracture surfaces for (a) Cast-A, (b) PM-X and (c) PM-Y 60-NITINOL materials in the water-quenched heat treatment condition showing the fracture origins (FO) and features characteristic of intragranular brittle fracture.

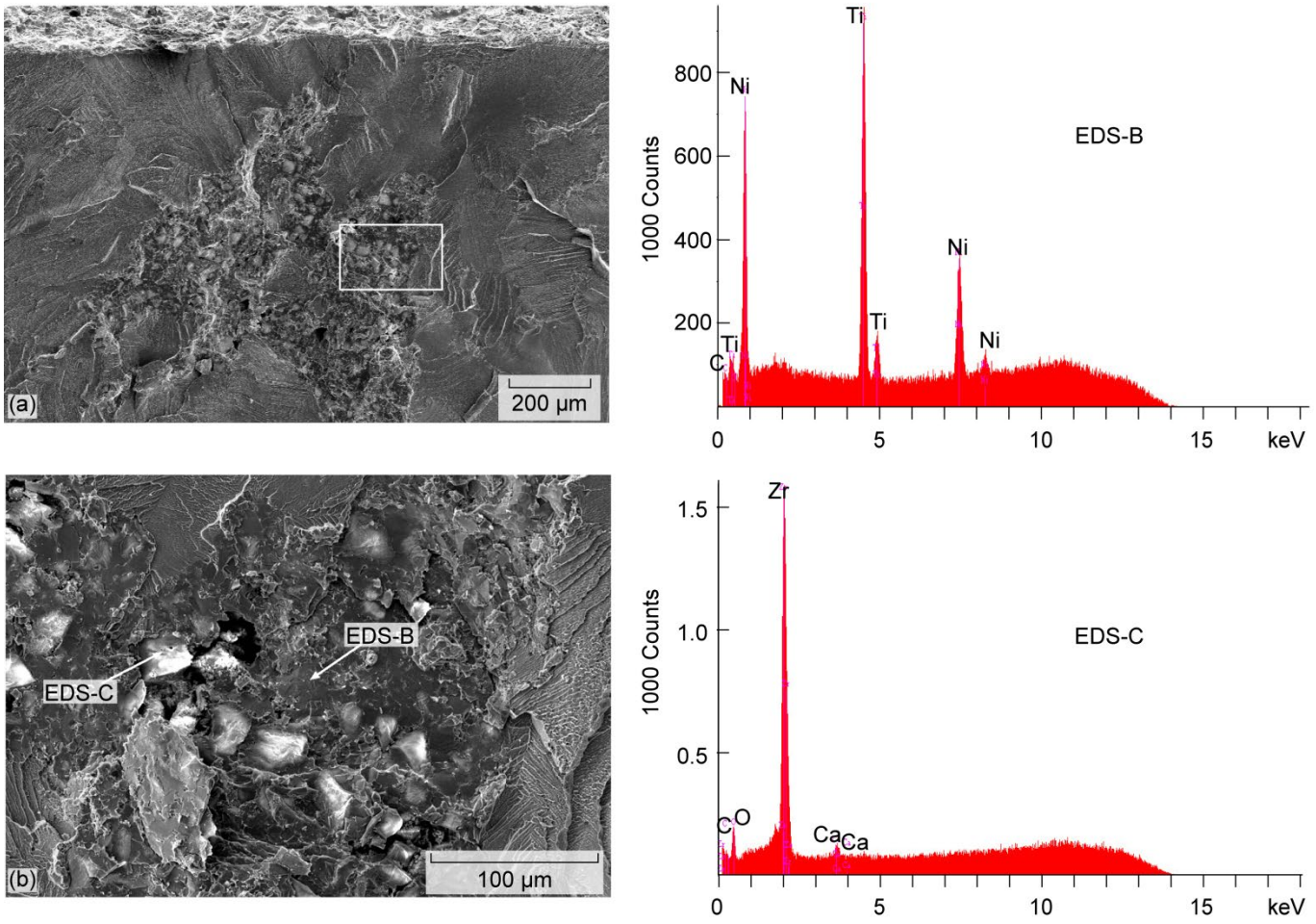

Figure 10.—Contamination in water-quenched Cast-A material in the water-quenched heat treatment condition. The highlighted area in *a* is shown at higher magnification in *b*. *EDS-B* represents the parent material (60-NITINOL), while *EDS-C* indicates that the particulate contaminant is composed of Zr and O.

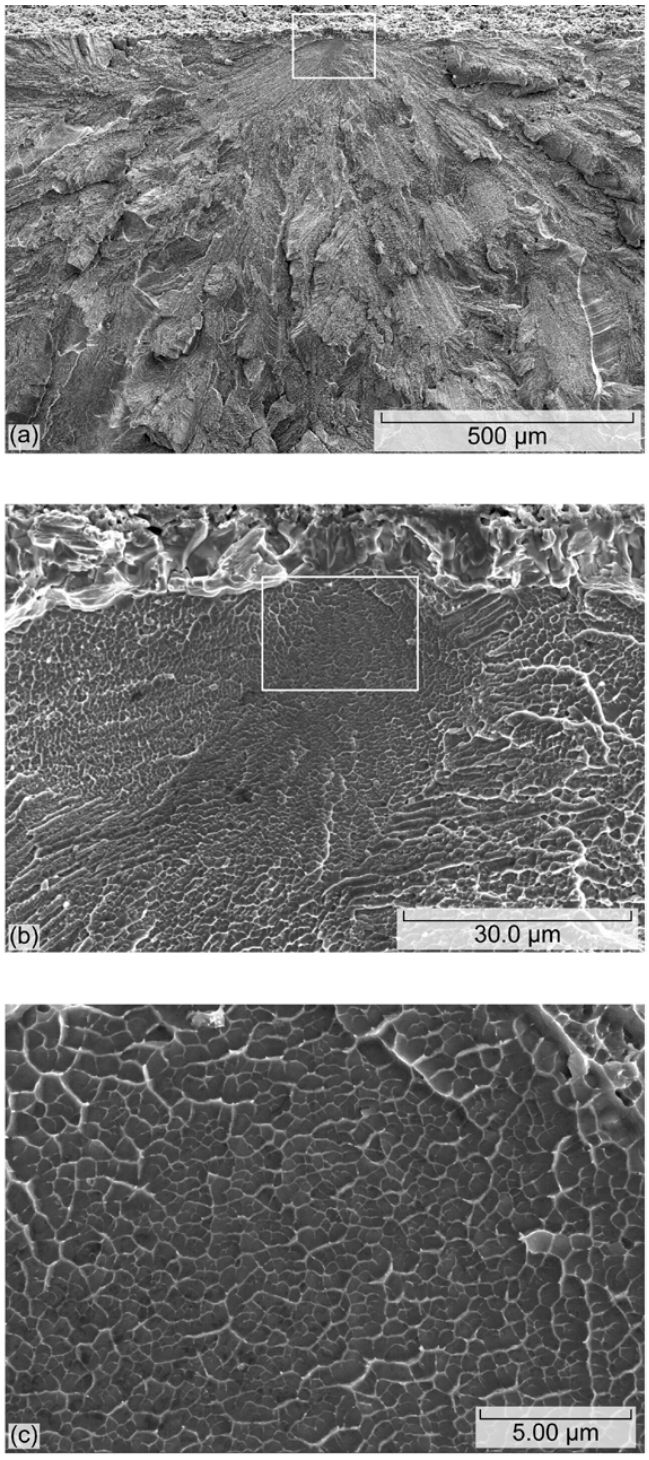

Figure 11.—SEM photomicrograph of the fracture surface (a), the fracture initiation site (b) and a higher magnification image of the fracture initiation site (c) of a PM-Y Charpy specimen in the water-quenched heat treatment condition. Note the fibrous texture at the fracture initiation site, an indication of (micro-scale) ductility.

Higher-magnification images of the fracture surfaces of the water-quenched PM-Y material, shown in Figure 11 show slight indications of ductile fracture where the material displays a fibrous texture. This finding was quite surprising, given the brittle nature of intermetallics, and it indicates that the material had some ductility and yielded prior to failure.

The fracture surfaces of the aged specimens, shown in Figure 12, were basically identical to those of the water-quenched specimens by the examination methods used in this study. Examination of the grainy contaminant in the Cast-A material seen in Figure 13 again showed that the contaminant consisted of Zr and O, as described in Figure 14 and Figure 15. Chemical analysis by ICP-OES showed that the chemical composition at the fracture origin consisted of 20 ppm Zr. No Zr was detected in the bulk material analysis, as listed in Table II, primarily because the contamination is sparsely distributed throughout the parent material but concentrated at fracture origins. This contamination increases the likelihood of fracture initiation since the particles are sharply faceted. As seen in Figure 13, the ZrO_2 contaminant in the aged Cast-A material appears to be less integrated with the parent material than in the Cast-A water-quenched material (see, for example, Figure 10(b)). It is possible that the contaminant particles remain trapped in the parent material after the water-quenching treatment but the aging treatment allows some subsequent residual stress relaxation, resulting in free-standing particles. Examination of a cross-section of the aged Cast-A specimen (shown in Figure 16) revealed further indication of contamination, which was found to be TiN (see Figure 17). This could be the result of some exposure to air during the casting process.

The fracture surface of the aged Cast-B specimen, shown in Figure 18, displays indications of brittle fracture as with the Cast-A specimens (e.g., Figure 13). An etched cross-section of this specimen (Figure 19) shows second phase Ni_3Ti generally clustered near the grain boundaries.

Examination of the fracture origin of a PM-X specimen revealed faceted unconsolidated particles at the fracture origin, as shown in Figure 20. This is further evidence that unconsolidated particles are a factor in the fracture of this material, whether by reducing the energy required for fracture initiation or that for crack propagation. A cross-section of this specimen (Figure 21) also showed several unconsolidated particles.

Figure 22 shows photomicrographs of the fracture surface and a metallographic cross-section of an aged PM-Y specimen. The relatively flat fracture initiation site is at the center of the divergence of the river patterns and is indicative of brittle transgranular fracture. The microstructure (Figure 22(b)) also indicates that fracture was transgranular and that the material was well-consolidated with some indications of prior particle boundaries.

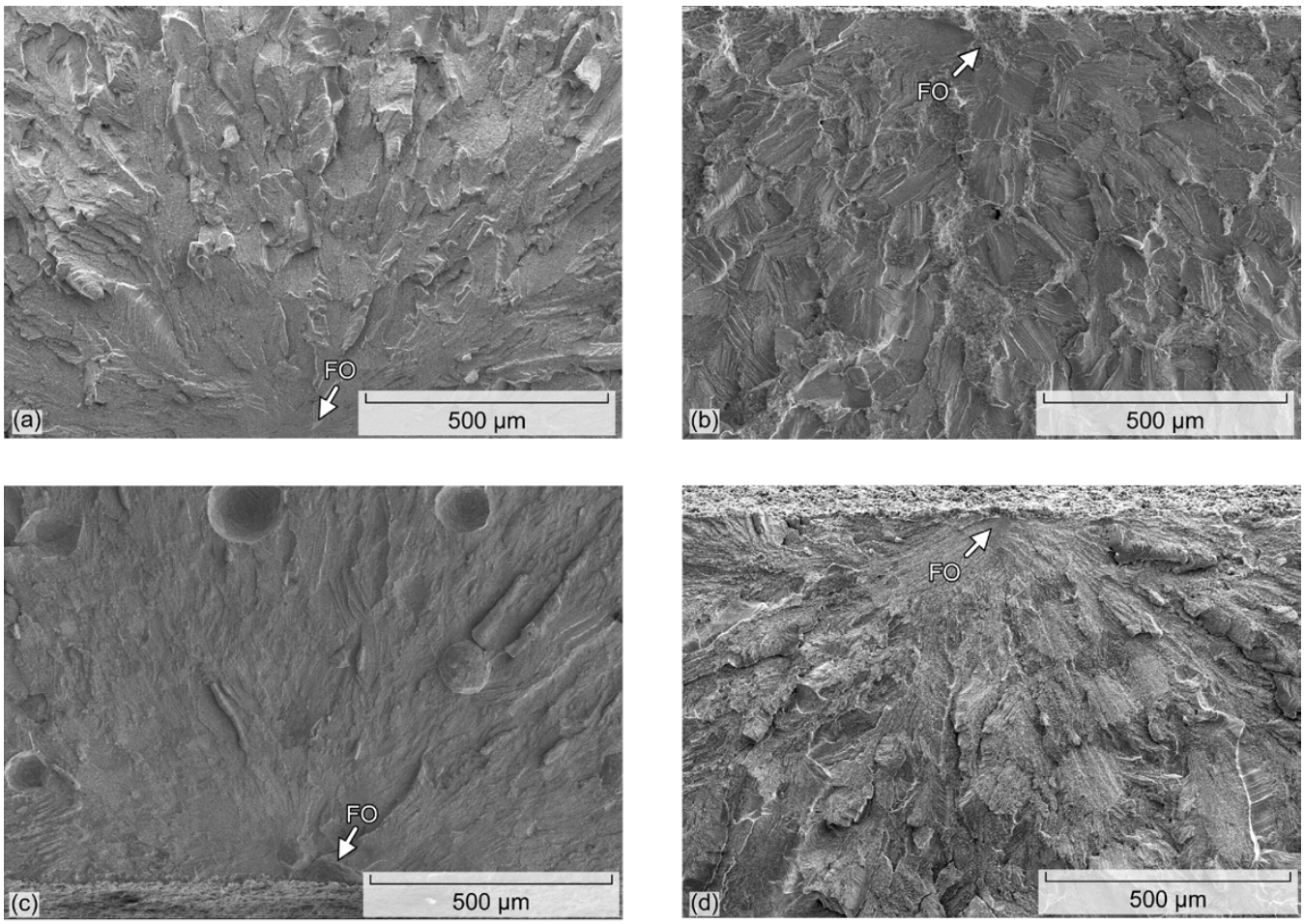

Figure 12.—SEM photomicrographs of representative fracture surfaces for (a) Cast-A, (b) Cast-B, (c) PM-X and (d) PM-Y 60-NITINOL materials in the aged heat treatment condition showing the fracture origins (FO).

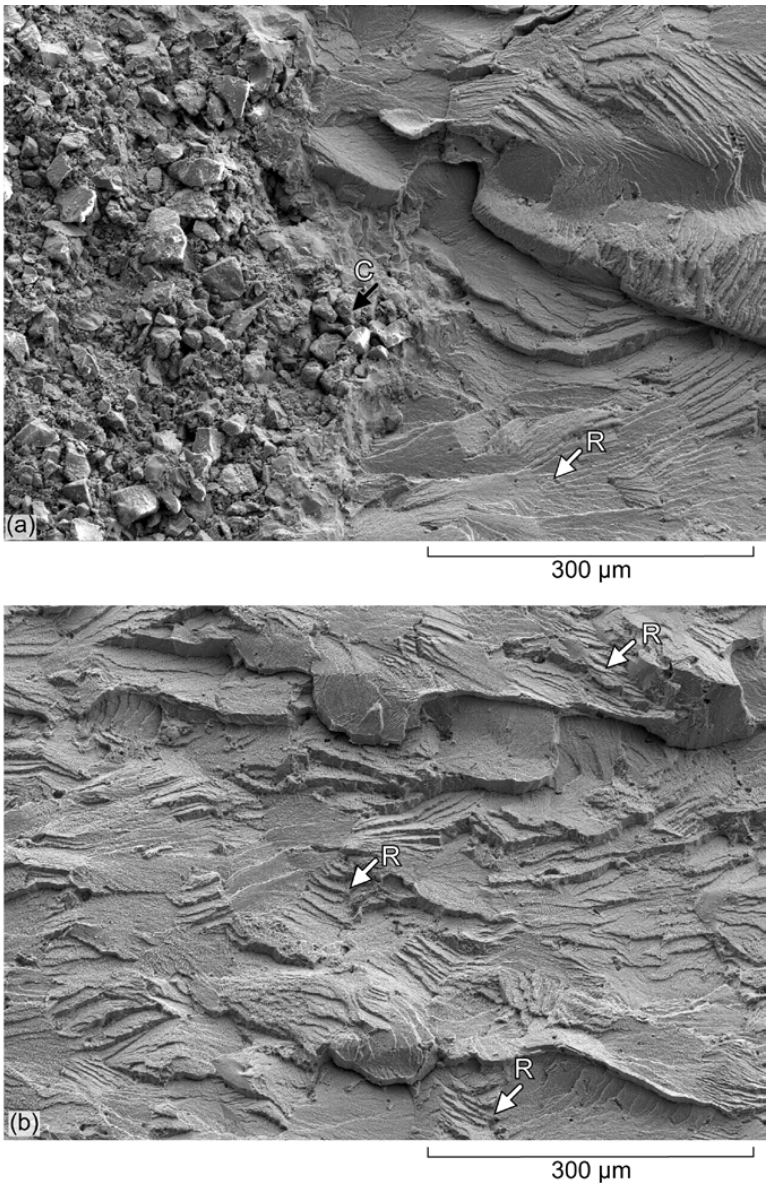

Figure 13.—Fracture origin and adjacent fracture surface for aged Cast-A specimen showing river patterns (R) indicating brittle fracture and particulate contamination (C) at fracture origin.

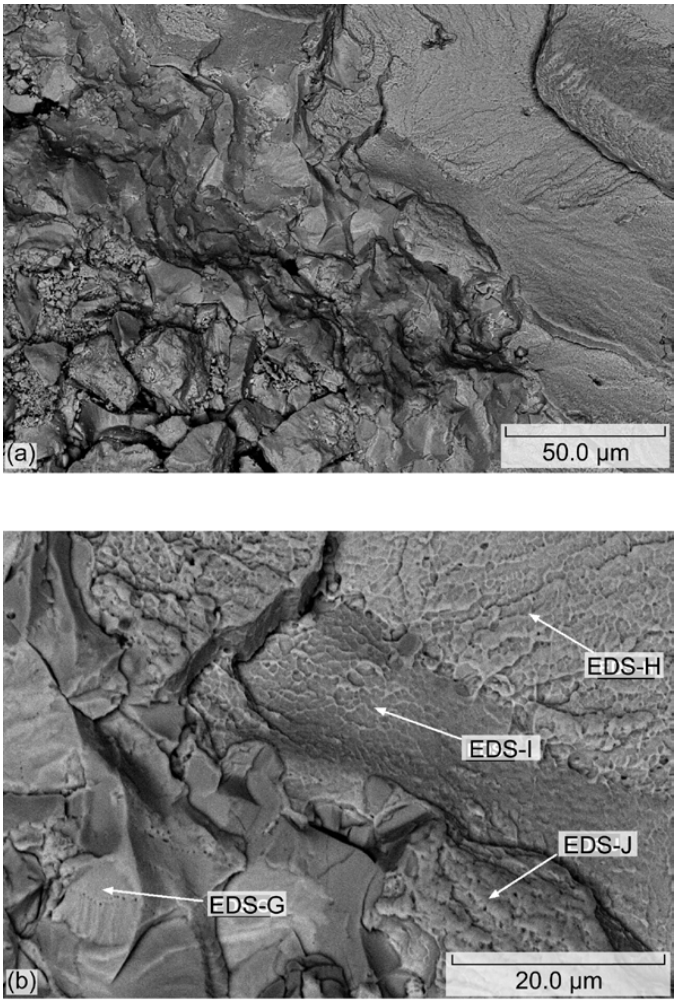

Figure 14.—Backscattered electron images at (a) low- and (b) high-magnification at edge of fracture origin in a Cast-A specimen. EDS spectra are shown in the following figure, indicate that the contamination is zirconia, while the parent material is Ni-Ti.

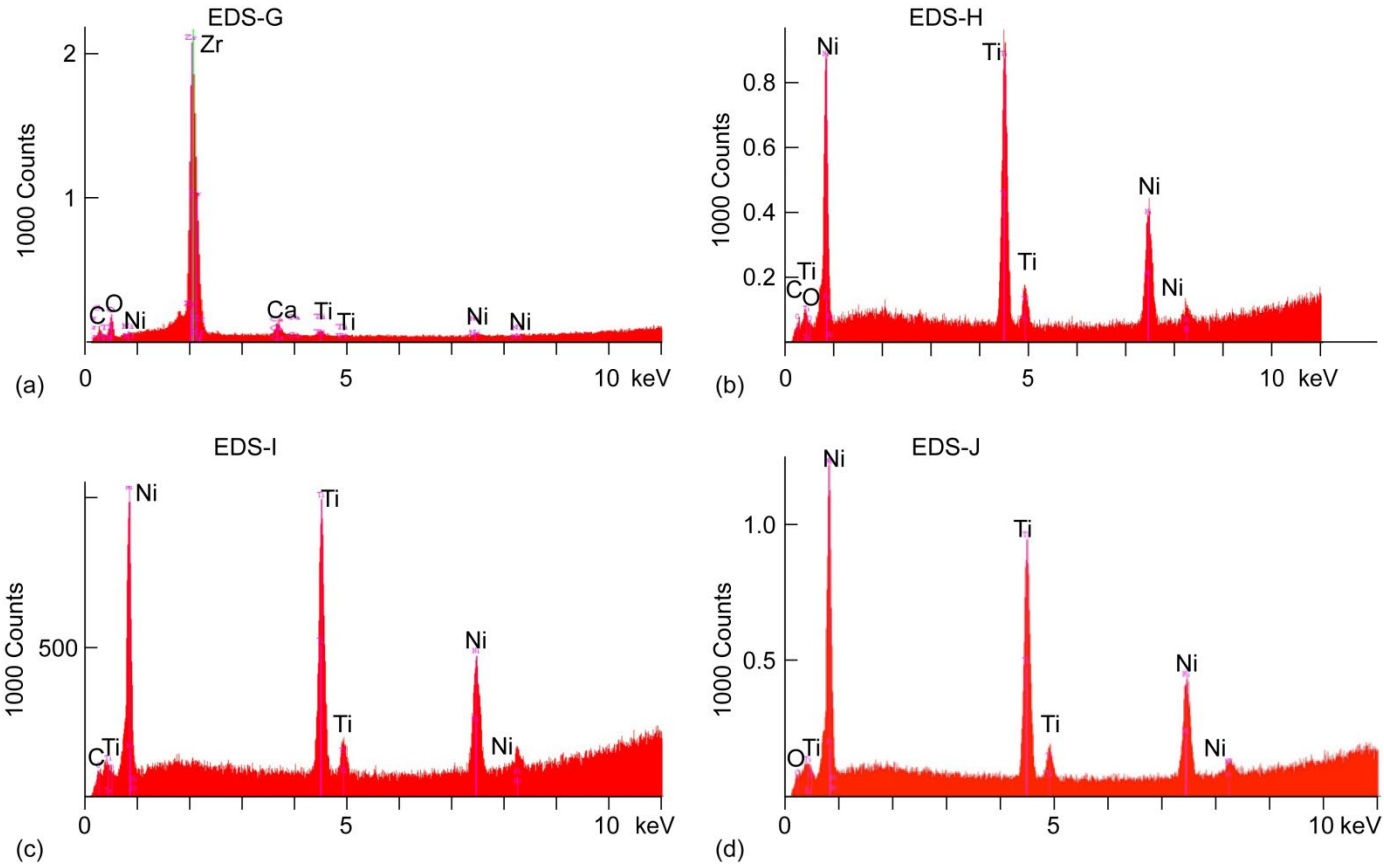

Figure 15.—EDS spectra from Figure 14 showing that the contamination (a) is primarily Zr and O, while the parent material (b) as well as the transition region (c) and (d) is Ni and Ti.

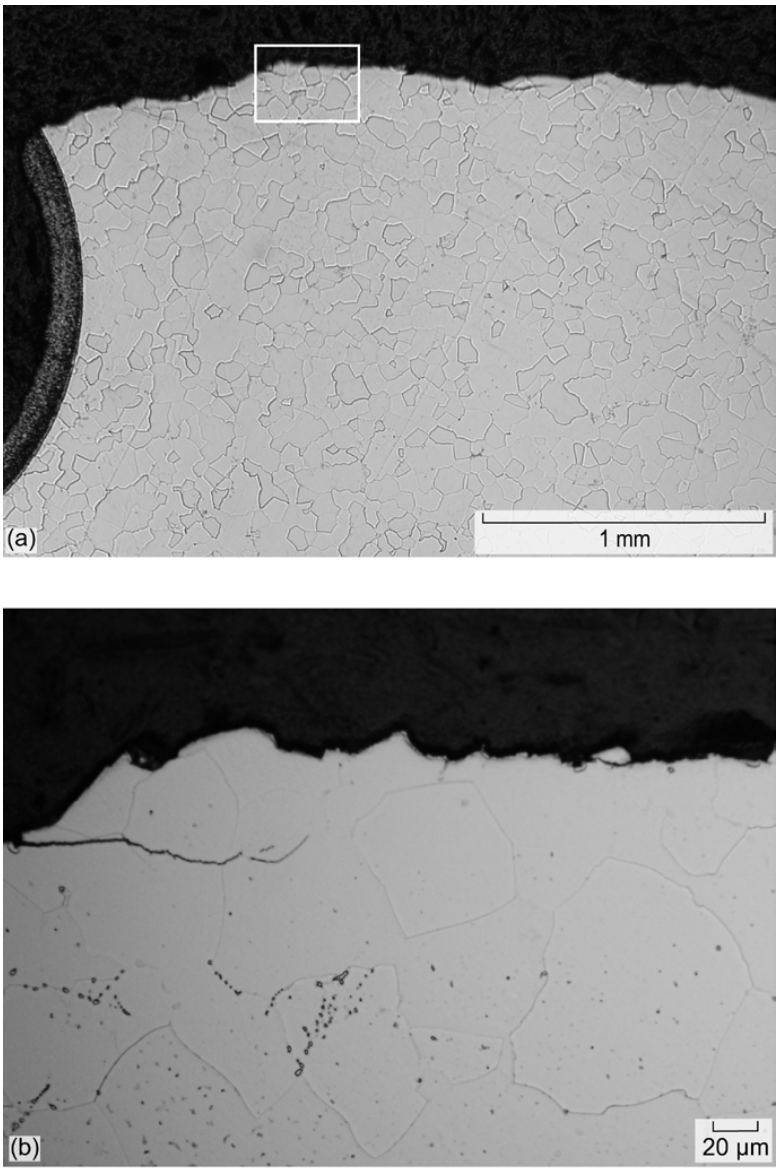

Figure 16.—Cross-section of aged Cast-A specimen (a) perpendicular to fracture surface and (b) at higher magnification showing intragranular fracture and an unexpected precipitate phase within the grains.

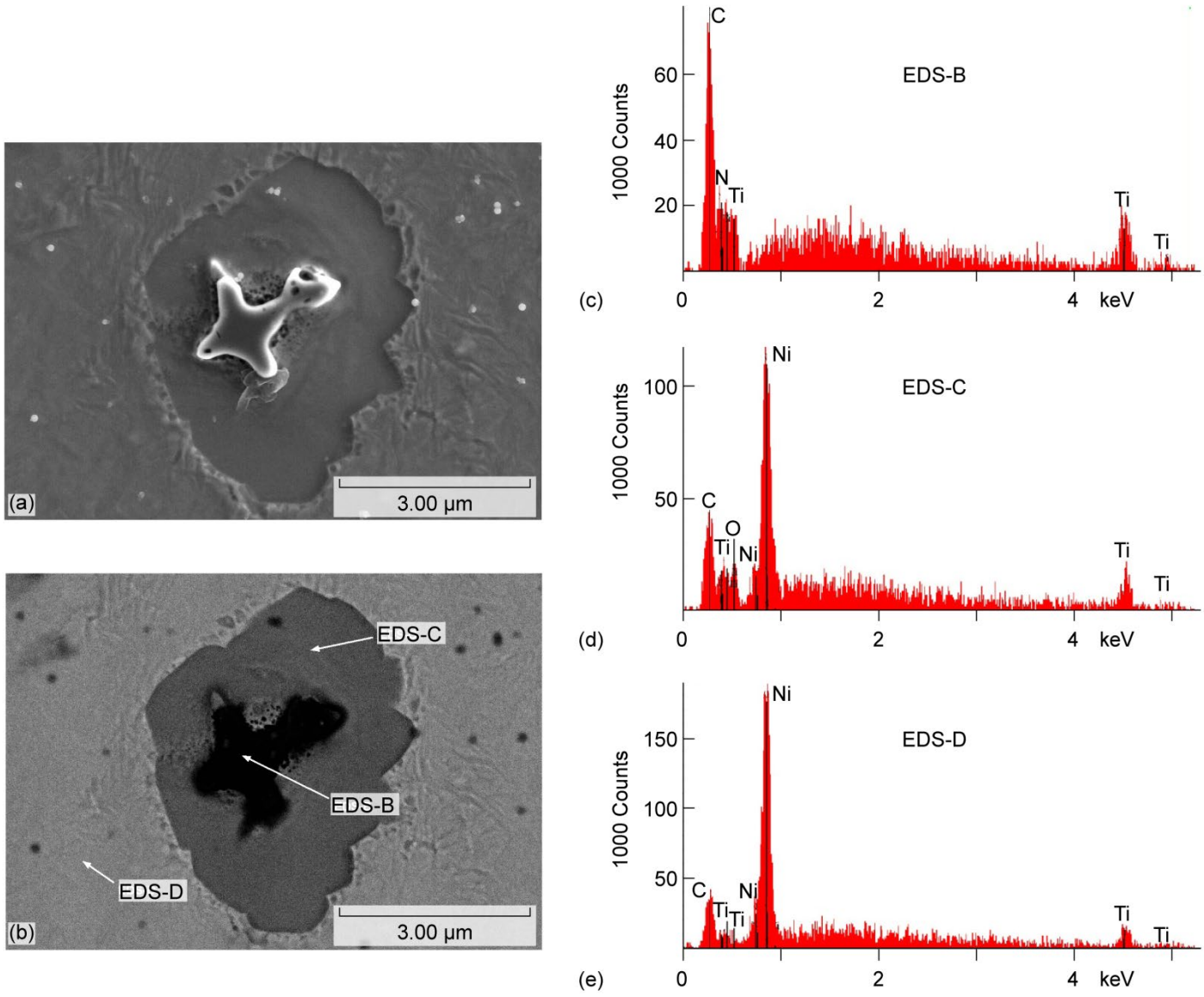

Figure 17.—(a) Secondary electron and (b) backscattered electron SEM images and accompanying EDS spectra ((c) to (e)) of one of the second phase features within the grains of an aged Cast-A Charpy specimen indicating that this feature is a contaminant composed of TiN (EDS-C) and TiC (EDS-D).

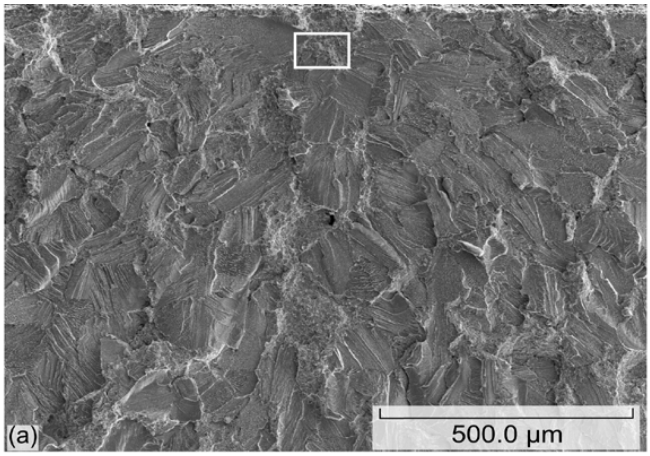

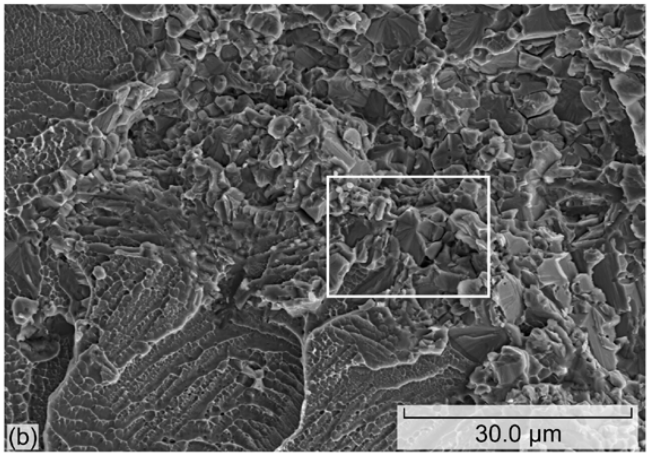

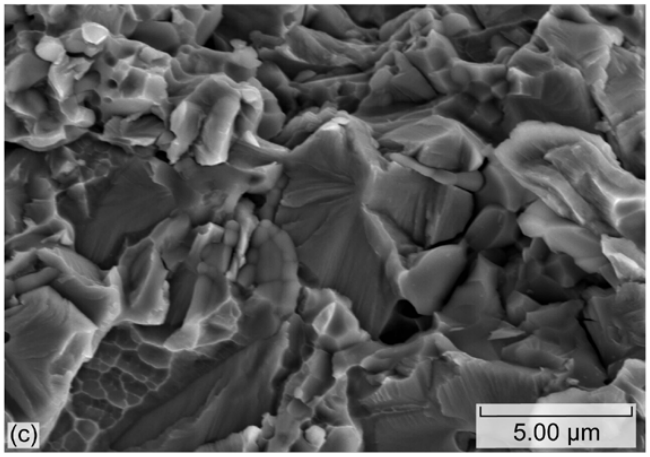

Figure 18.—Fracture surface of aged Cast-B with microstructural features indicating brittle fracture. The highlighted area in (a) is shown at higher magnification in (b) and likewise for the highlighted area in (b).

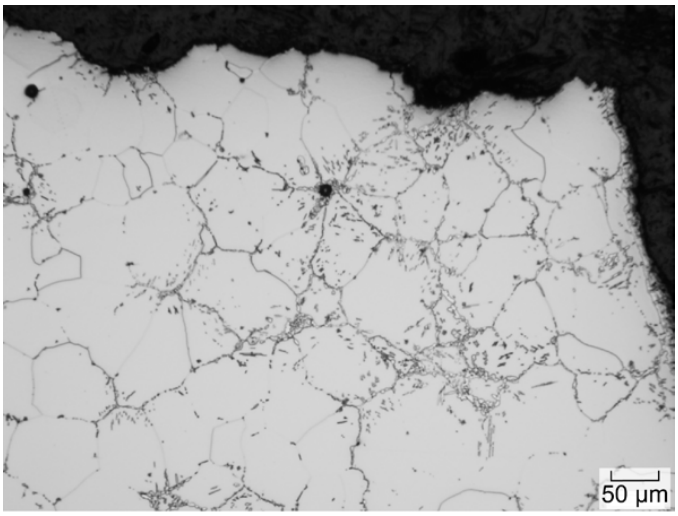

Figure 19.—Cross-section of aged Cast-B specimen through fracture surface (U-notch on right).

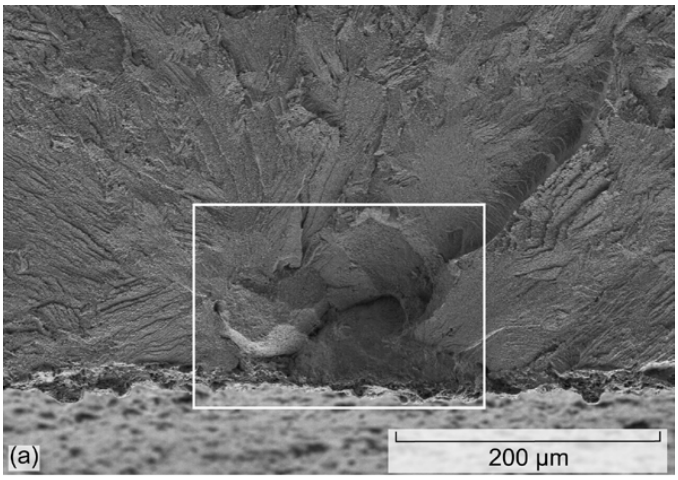

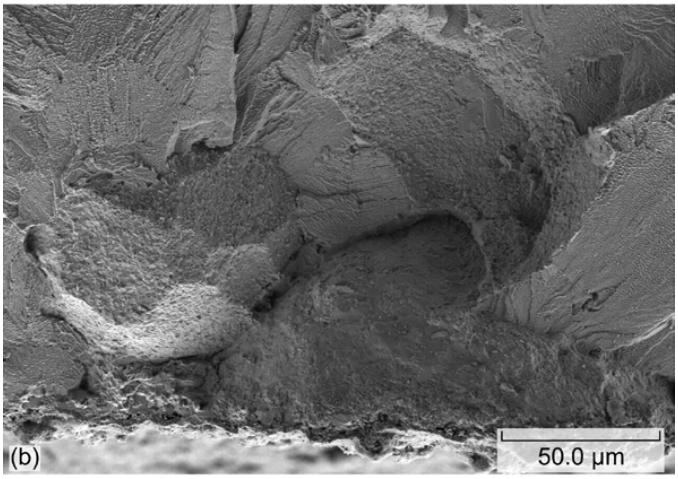

Figure 20.—Unconsolidated particles at the fracture origin of a PM-X Charpy specimen in the aged heat treatment condition

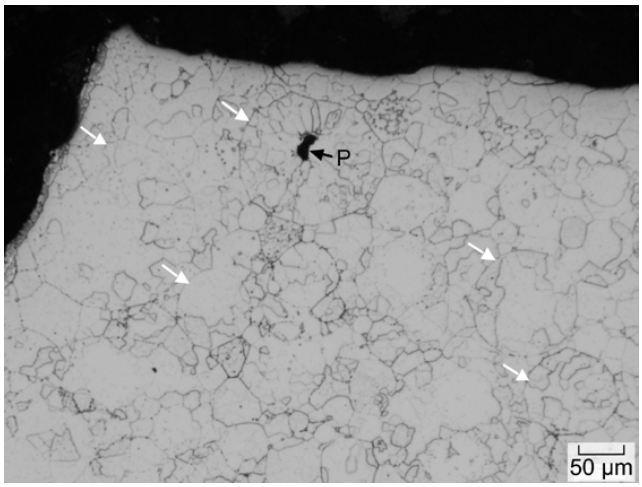

Figure 21.—Cross section of aged PM-X through U-notch, near fracture surface. Several unconsolidated particles are called out with arrows. The pore at P is likely the product of a particle with a hollow core.

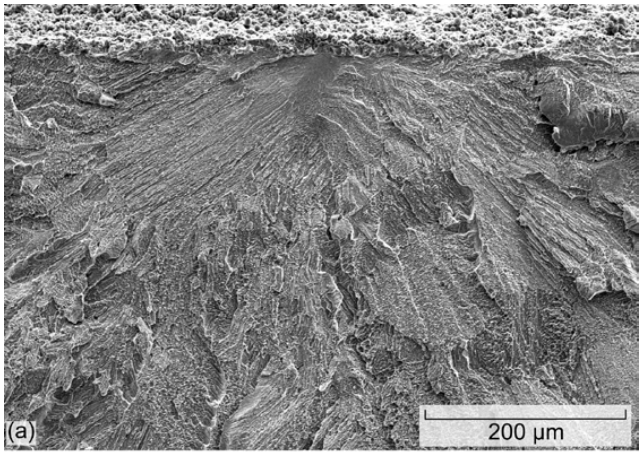

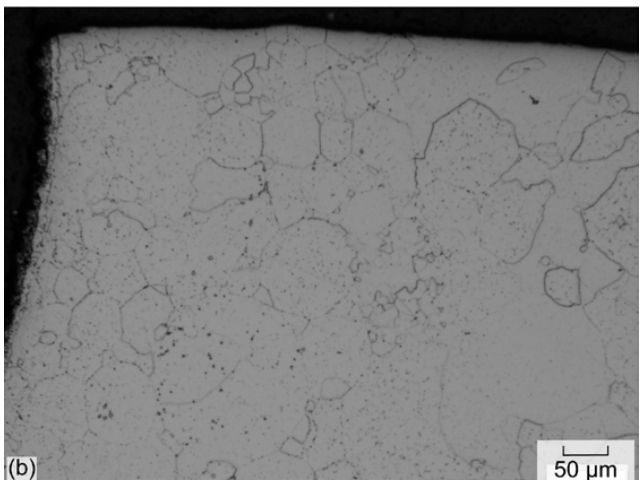

Figure 22.—(a) SEM of the fracture surface and (b) optical photomicrograph of a cross-section through the U-notch of a Charpy specimen fabricated from PM-Y in the aged heat treated condition.

Hardness and Impact Energy

The impact energy results are listed in Table III. The tabulated values are the average and standard deviation of three to four replicate specimens. The aged and water-quenched specimens had average impact energies of 0.43 ± 0.04 and 0.39 ± 0.08 J, respectively. Based on the stated statistical variation of the averages for the studies specimens, there was essentially no difference between the impact energies of materials heat treated by these two methods. The furnace-cooled specimens, however, had an average impact energy of 1.02 ± 0.14 J, more than twice that of either aged or water-quenched specimens. While this difference in impact energy is significant with respect to the effect of the studied heat treatments on this 60-NITINOL, it should be noted that the impact energy of this material is between that of metallic and ceramic materials used in bearings. Examples of the impact energies of such materials are listed in Table IV.

The microindentation hardness results are shown in Table III. These values represent the average and standard deviation of five repeat measurements, approximately 500 µm apart. The data shows that the hardness is highest for the water-quenched and aged specimens. The aged and water-quenched specimens had average hardness values of 641 ± 42 and 664 ± 19 HV, respectively. The furnace-cooled specimens had an average hardness value of 324 ± 39 HV, approximately half that of either the aged or water-quenched specimens Based on the given statistical variation, there is no difference in the hardness values for specimens with either the water-quenched or aged heat treatment conditions. There was also no difference in hardness for water-quenched specimens whether they were made by the casting method or by PM. The difference between hardness values of aged specimens fabricated by different processing methods was approximately 6 percent.

The results indicate an inverse relationship between impact energy and hardness for this material, regardless of the processing method. This finding may enable the selection of a heat treatment process that optimizes hardness and impact resistance. The salient issue, however, is that the impact resistance of this material is relatively low due to its inherent brittleness. Table IV lists the impact energies of several engineered materials, including 60-NITINOL. Clearly, the impact energy of 60-NITINOL is low compared to metallic bearing materials (e.g., 440C and M50), but in the notched condition the impact energy of this material is significantly higher than that of many of the engineered ceramics that are now used in full ceramic bearings. In fact, the impact energy of 60-NITINOL is close to that of partially stabilized zirconia (ZrO_2 – 3mol% Y_2O_3), though the impact energy of zirconia listed in Table IV was obtained from an unnotched specimen. Careful consideration of the property trade-offs for this material will be necessary for its successful implementation in aerospace components.

TABLE III.—IMPACT ENERGY AND MICROINDENTATION HARDNESS RESULTS.
[Data for conditions that were not available are listed N/A.]

	Impact energy, J				Microindentation hardness, HV_{500}			
Heat treatment↓\ Designation→	Cast-A	Cast-B	PM-X	PM-Y	Cast-A	Cast-B	PM-X	PM-Y
Water-quenched	0.37±0.004	N/A	0.33±0.04	0.49±0.06	673.5±17.2	N/A	675.5±11.7	641.6±18.3
Aged	0.48±0.02	0.45±0.05	0.39±0.02	0.41±0.02	630.7±16.6	589.8±5.7	692.3±14.1	650.2±12.9
Annealed	1.00±0.03	N/A	0.89±0.03	1.18±0.04	288.6±13.8	N/A	365.7±17.8	318.5±7.4

TABLE IV.—IMPACT TEST RESULTS COMPARED TO OTHER ENGINEERED MATERIALS AND TO EXTRUDED AND HARDENED 60-NITINOL

Material	Impact Energy, J
L2 tool steel (Ref. 17)	26
410 stainless steel (Ref. 17)	34
Extruded 60-NITINOL (Ref. 18)	6.8 (notched)
Hardened 60-NITINOL (Ref. 18)	2.7 (notched)
Cast 60-NITINOL:	
Furnace-cooled	1.0 (notched)
Water-quenched	0.4 (notched)
Aged	0.5 (notched)
Partially stabilized ZrO_2 (Ref. 19)	0.9 (unnotched)
Cold isostatically pressed and sintered Al_2O_3 (Ref. 20)	0.1 (unnotched)
Sintered SiC (Ref. 21)	0.1 (unnotched)
Sintered and HIPped Si_3N_4 (Ref. 22)	0.08 (unnotched) 0.01 (notched)

Conclusions

The impact energy and hardness of 60-NITINOL fabricated by casting and by powder metallurgy techniques and subjected to various heat treatments has been studied. Based on the results of this study, the following conclusions can be drawn:

1. The impact energy of 60-NITINOL after either the water-quenching or aging heat treatments is approximately half that of the material after furnace annealing.
2. The hardness of 60-NITINOL after either water-quenching or aging is approximately twice that of the material after furnace annealing.
3. There is an inverse relationship between impact resistance and hardness of this material, which suggests possible selection of heat treatments for optimum properties.
4. The impact energy of 60-NITINOL is intermediate to that of conventional metallic bearing materials and typical advanced ceramic bearing materials, being most comparable to partially stabilized zirconia.

References

1. Sides, Hampton, "The Titanic, Illuminated," National Geographic, Vol. 221, No. 4, pp. 78-109, April 2012.
2. R.W. Hertzberg, Deformation and Fracture Mechanics of Engineering Materials, 4th ed., John Wiley & Sons, New York, 1996.
3. "A Titan of the World," in *Titanic: the Tragedy that Shook the World*, Robert J. Sullivan, ed., Life Books, New York, Vol. 12, No. 4, pp. 46-65, March 23, 2012.
4. Pedersen, P.T., Zhang, S., 1998. On impact mechanics in ship collisions. J. Mar. Struct.11 (10), 429–449.
5. Løset, S., Kvamsdal, T., 1994. Iceberg/structure interaction-effects of ice temperature on the impact force. Proc. of the Int. Association for Hydro-Environment Eng. And Research (IAHR) Ice Symposium, Trondheim, Norway, pp. 205–218.
6. Liu, Z., Amdahl, J., 2010. A new formulation of the impact mechanics of ship collisions and its application to a ship–iceberg collision. J. Mar. Struct. 23 (3), 360–384.
7. Nicholas, T., Barber, J.P., and Bertke, R.S., 1980. Impact damage on titanium leading edges from small hard objects. Exp. Mech. 20, 357–364.
8. Chen, X. and Hutchinson, J.W., "Particle impact on metal substrates with application to foreign object damage to aircraft engines," Journal of the Mechanics and Physics of Solids 50 (2002) 2669–2690.
9. A.F. Dericioglu, S. Zhu, Y. Kagawa and H. Kasano, "Damage Behavior of Air Plasma Sprayed Thermal Barrier Coatings under Foreign Object Impact," Advanced Engineering Materials, 2003, Vol. 5, No. 10, pp. 735-37.
10. F. Abdi, K. Bowcutt, C. Godines and J. Bayandor, "Collision Provoked Failure Sequencing in Space Reentry Vehicles," Computers and Structures, 2011, Vol. 89, pp. 930-39.
11. I. Ye. Telitchev, L.G. Lukashev and A.G. Prokhorov, "Residual Toughness of Space Vehicles Structural Elements Damaged by Space Debris," Int. J. Impact Engng., Vol. 20, pp. 789-800, 1997.
12. C. DellaCorte, S.V. Pepper, R. Noebe, D.R. Hull, G. Glennon, "Intermetallic Nickel-Titanium Alloys for Oil-Lubricated Bearing Applications," NASA/TM—2009-

215646, March 2009, National Technical Information Service, Springfield, VA.
13. C. DellaCorte, R.D. Noebe, M.K. Stanford, S.A. Padula, "Resilient and Corrosion-Proof Rolling Element Bearings Made From Superelastic Ni-Ti Alloys for Aerospace Mechanism Applications," NASA/TM—2011-217105, September 2011, National Technical Information Service, Springfield, VA.
14. ASTM Designation E 23-07a$^{\varepsilon 1}$, "Standard Test Method for Notched Bar Impact Testing of Metallic Materials," 2010, vol. 03.01, American Society for Testing and Materials, West Conshokocken, PA.
15. ASTM Designation E 384-11$^{\varepsilon 1}$, "Standard Test Method for Knoop and Vickers Hardness of Materials," 2011, vol. 03.01, American Society for Testing and Materials, West Conshokocken, PA.
16. M.K. Stanford, F. Thomas and C. DellaCorte, "Processing Issues for Preliminary Melts of the Intermetallic Compound 60-NITINOL," NASA/TM-201X-216044, 201X, in publication.
17. J.F. Shakelford, *Introduction to Materials Science for Engineers*, Sixth Edition, 2005, Prentice-Hall, Upper Saddle River, NJ.
18. W.J. Buehler, "Intermetallic Compound Based Materials for Structural Applications," in *The Seventh Navy Science Symposium: Solution to Navy Problems through Advanced Technology, May 14, 15, 16, 1963, U.S. Naval Aviation Medical Center, Pensacola, Florida. Vol. 1*, Office of Naval Research, Arlington, VA, 16 May 1963.
19. T. Kobayashi, M. Niinomi, Y. Koide and K. Matsunuma, "Instrumented Impact Testing of Ceramics," Transactions of the Japan Institute of Metals, Vol. 27, No. 10, p. 775-783, 1986.
20. R.L. Bertolotti, "Strength and Adsorbed Energy in Instrumented Impact Tests of Polycrystalline Al_2O_3," *Journal of the American Ceramic Society*, Vol. 57, No. 7, pp. 300-302, July 1974.
21. H.C. Chandan, L. Hermansson, H. Abe and R.C. Bradt, "Elevated Temperature Instrumented Charpy Impact of a Sintered Silicon Carbide," *Ceramics International*, Vol. 9, No. 4, pp. 114-118, Oct-Dec 1983.
22. M.B. Maros, N. Kaulics, P. Arató, "Characterization of Dynamic Failure Process of Si3N4 ceramics, Part I: Test Procedures, Fracture Energies, and Fractographic Analysis," *Ceramic Transactions*, Vol. 199, pp. 421-433, 2007.